Neuron, Vol. 17, 945–956, November, 1996, Copyright ©1996 by Cell Press

Enhanced LTP in Mice Deficient in the AMPA Receptor GluR2

Zhengping Jia,*§ Nadia Agopyan,*§ Peter Miu,† Zhigang Xiong,‡ Jeff Henderson,* Robert Gerlai,* Franco A. Taverna,* Alexander Velumian,† John MacDonald,‡ Peter Carlen,† Wanda Abramow-Newerly,* and John Roder*
*Samuel Lunenfeld Research Institute
Mount Sinai Hospital
600 University Avenue
Toronto, Ontario M5G 1X5
†Playfair Neuroscience Unit
Toronto Hospital
Toronto, Ontario
‡Department of Physiology
University of Toronto
Toronto, Ontario

Summary

AMPA receptors (AMPARs) are not thought to be involved in the induction of long-term potentiation (LTP), but may be involved in its expression via second messenger pathways. However, one subunit of the AMPARs, GluR2, is also known to control Ca^{2+} influx. To test whether GluR2 plays any role in the induction of LTP, we generated mice that lacked this subunit. In GluR2 mutants, LTP in the CA1 region of hippocampal slices was markedly enhanced (2-fold) and nonsaturating, whereas neuronal excitability and paired-pulse facilitation were normal. The 9-fold increase in Ca^{2+} permeability, in response to kainate application, suggests one possible mechanism for enhanced LTP. Mutant mice exhibited increased mortality, and those surviving showed reduced exploration and impaired motor coordination. These results suggest an important role for GluR2 in regulating synaptic plasticity and behavior.

Introduction

In the mammalian CNS, α-amino-3-hydroxy-5-methyl-4-isoxazolepropionate (AMPA) receptor subtypes of the glutamate receptors are the principal mediators of fast excitatory synaptic transmission. Four genes, GluR1, 2, 3, and 4 (also called GluRA, B, C, and D) encode heteromeric receptors with high affinity for AMPA, but low affinity for kainic acid (Hollmann and Heinemann, 1994). The relative levels of expression of these genes, as well as splicing and editing of their mRNAs, account for the wide differences in Ca^{2+} permeability and gating between cells (Geiger et al., 1995). Homomeric channels, assembled from GluR2 subunits, are not permeable to Ca^{2+} and showed outwardly rectifying current/voltage (I/V) relations. In contrast, receptors assembled from GluR1, GluR3, and GluR4 subunits are highly permeable to Ca^{2+}, and showed a doubly rectifying I/V relation (Hollmann et al., 1991; Verdoorn et al., 1991). Comparison of the amino acid sequence of the GluR2 subunit with that of the other subunits revealed a positively charged arginine (R) at position 586 of the transmembrane segment 2, instead of the neutral glutamine (Q) found at the homologous position in the other subunits. This position, termed the Q/R site, was subject to RNA editing (Sommer et al., 1991) and is the main site controlling divalent ion permeation of recombinant AMPA receptors (AMPARs) (Hume et al., 1991; Burnashev et al., 1992a; Dingledine et al., 1992). Coexpression of the GluR2 subunit with GluR1, 3, and 4 showed that AMPARs containing the Q/R edited GluR2 subunit exhibited lower Ca^{2+} permeability and outwardly rectifying I/V relationships. Conversely, overexpression of unedited GluR2 yielded higher Ca^{2+} permeability in the neurons of gene-targeted mice (Brusa et al., 1995). The studies indicate that the channel properties of the GluR2 subunit dominate those of the heteromeric receptor complex. Therefore, one would predict that Ca^{2+} permeability in the CNS could be controlled by regulating expression of the GluR2 subunit. Indeed, the relative abundance of GluR2 mRNA correlates negatively with the Ca^{2+} permeability of native AMPARs in brain slices (Geiger et al., 1995). Thus, in principal neurons of the hippocampus (i.e., pyramidal and granule neurons), where GluR2 is highly expressed, AMPARs exhibit low Ca^{2+} permeability, whereas in cerebellar Bergman glial cells (Burnashev et al., 1992b), hippocampal basket cells, and neocortical nonpyramidal cells (Koh et al., 1995a), where expression of GluR2 is low or absent, AMPARs show higher Ca^{2+} permeability.

While these data clearly show the dominant role of the GluR2 subunit in inhibiting Ca^{2+} influx via AMPARs, the functional consequence of Ca^{2+} entry through synaptically activated AMPARs remains unknown. Since Ca^{2+}-permeable AMPAR channels are blocked by intracellular polyamines (Kamboj et al., 1995; Koh et al., 1995b; Bowie and Mayer, 1995) at positive membrane potentials and N-methyl-D-aspartate (NMDA) receptor channels are blocked by extracellular Mg^{2+} at negative membrane potentials (MacDonald and Wojtowicz, 1982; Nowak et al., 1984), it was hypothesized that at excitatory synapses, where AMPARs and NMDA receptors are colocalized, Ca^{2+} influx through the AMPARs would be comparable with that through NMDARs at resting membrane potential (Burnashev et al., 1995). Thus, hyperpolarization would favor Ca^{2+} influx through AMPARs, and depolarization would favor Ca^{2+} influx through NMDA receptors, which has been implicated in long-term potentiation (LTP) (Bliss and Collingridge, 1993). However, the lack of specific AMPAR subunit antagonists has hindered studies that would elucidate the functional role of Ca^{2+} influx through the AMPARs. In an attempt to address the issue of whether Ca^{2+} influx through the AMPARs plays any modulatory role in synaptic transmission and synaptic plasticity, we have generated mutant mice lacking the GluR2 protein. Isolated hippocampal CA1 neurons showed enhanced Ca^{2+} permeation and LTP was markedly enhanced in hippocampal slices. While several knockouts have decreased LTP

§These authors contributed equally to this work.

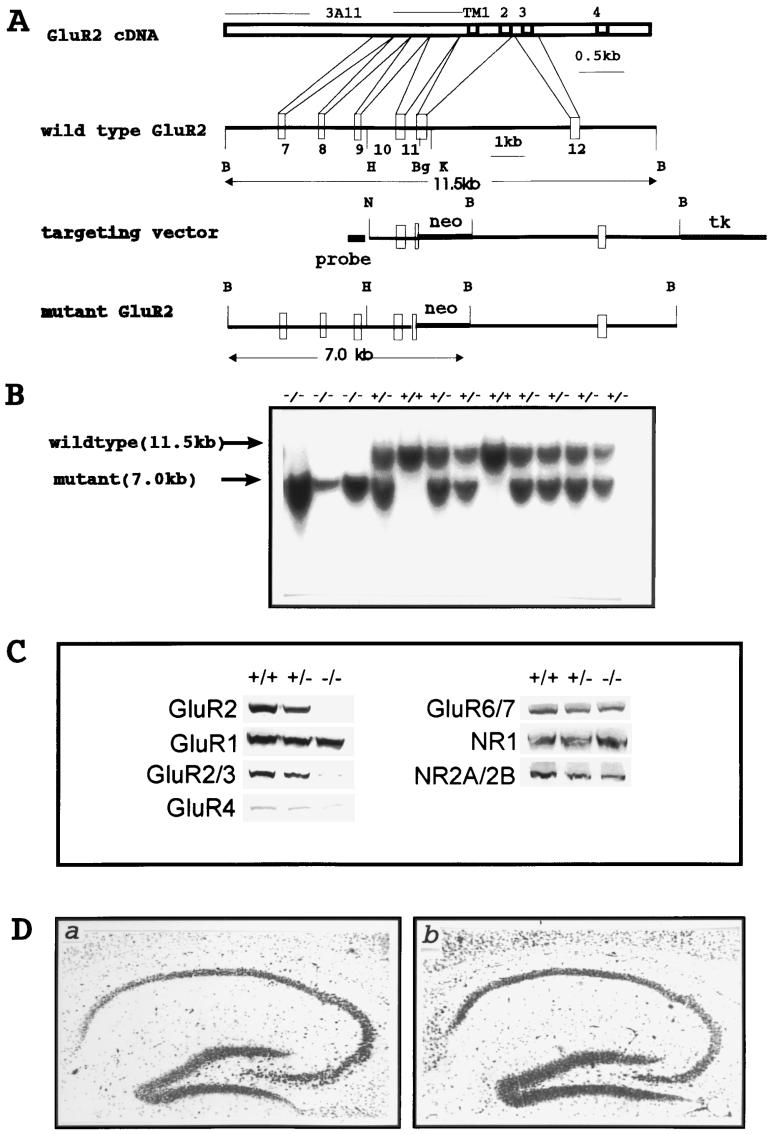

Figure 1. Targeted Disruption of the GluR2 Gene

(A) The GluR2 cDNA showing the hydrophobic membrane domains (TM) and the anti-GluR2 antibody epitope (3A111), the isogenic 129 strain genomic clone (exons, open boxes), targeting vector, and the mutant GluR2 locus expected following homologous recombination. B, BamHI; H, HindIII; Bg, BglII; K, KpnI; N, NotI.

(B) Southern blot analysis of genomic DNA isolated from the tails of a representative F2 litter of 12 mice derived from a heterozygous (+/−) 129 × CD1 F1 inter-cross. DNA was digested with BamHI and probed with a 0.4 kb fragment 5′ to exon 10, yielding diagnostic 11.5 kb restriction fragments from wild type (+/+) and 7.0 kb from mutant alleles (−/−).

(C) Western blot analysis. Brain plasma membrane proteins were loaded at 50 μg per lane and probed with the antibodies indicated.

(D) Sagittal sections of hippocampus from −/− (left) or +/+ (right) mice, stained with Cresyl violet. Serial sections in the coronal, sagittal, and horizontal planes of the entire CNS of wild-type (n = 2) and GluR2$^{-/-}$ mutant (n = 2) mice revealed no difference in cellular morphology or in the organization and extent of fiber tracts (see Experimental Procedures). Staining with cytochrome C oxidase, a gross measure of presynaptic input, was also normal in mutants.

(e.g., Silva et al., 1992), this is the first knockout showing elevated LTP and behavioral abnormalities associated with it. Our data raise the possibility that Ca^{2+} influx via AMPARs alone may be able to induce long-lasting increases in synaptic efficacy, suggesting an important and unexpected role in synaptic plasticity.

Results

Targeted Disruption of the GluR2 Gene

To disrupt the GluR2 locus, an isogenic targeting vector was designed to delete transmembrane region 1 and the pore loop, which are essential for receptor function (Figure 1A) (Hollmann and Heinemann, 1994). R1 embryonic stem (ES) cells (strain 129) were electroporated with this vector and selected in G418 and gancyclovir (Nagy et al., 1993). Double resistant clones were screened for the desired homologous recombination by Southern blotting using a probe 5′ to exon 10 (Figure 1A). Four ES clones contained the targeting events, and were used to produce aggregation chimeras with CD1 morulae (Wood et al., 1993). Only one ES clone transmitted the GluR2 mutation through the germline. Heterozygous mice from a CD1 × 129 cross were intercrossed to produce 477 F2 offspring, of which 22% were +/+, 54% +/−, and 24% −/− (Figure 1B). This 1:2:1 Mendelian ratio suggests there was no embryonic lethality in the mutants. Mice from this cross were used in all experiments (see Figures 1–6), except that represented in Table 1. Western blot analysis of brain protein with a GluR2 antibody (3A11), produced against the N-terminal domain (Puchalski et al., 1994), showed no detectable GluR2 protein, either full-length (Figure 1C) or truncated, even at a 100-fold excess loading and a 1% level of detection (data not shown). Enhanced chemiluminescence (ECL) detection showed that +/− mice had ~50% ± 10% (n = 3) of GluR2 protein compared with +/+. In mutant mice, the level of the other glutamate receptors (GluR1, 4, 6, and 7; NMDAR1, 2A, and 2B) was not altered. Since there are no GluR3 antibodies

available, we used one that recognizes the C-terminus of both GluR2 and GluR3. GluR3 is known to be expressed at lower levels in brain than GluR2. As shown in Figure 1C, the lane from GluR2$^{-/-}$ mice showed a band indicating the presence of GluR3 in the GluR2 knockout mice. Based on the normal ratios of GluR2 and 3, it is unlikely that GluR3 is overexpressed, since the band is less intense than the GluR2 band. However, we cannot exclude the unlikely possibility that GluR3 is downregulated in the absence of GluR2. This experiment was repeated several times with similar results, using enriched synaptic membranes as well as whole-protein fractions from brain. Therefore, as best we can judge, the loss of GluR2 was selective and did not result in any developmental compensation or downregulation in other glutamate receptors. GluR2$^{-/-}$ mice were also found to possess all major neuroanatomic loci and fiber pathways in grossly normal proportion. The hippocampus exhibited normal cellularity in the CA regions 1–3 and dentate gyrus (Figure 1D). Golgi staining of the individual pyramidal neurons also revealed normal morphology. Fiber pathways within the hippocampus, such as the perforant path, also appeared normal, as did the structure of the cerebellum, the dorsal laminae of the spinal cord, and retina (data not shown).

General Appearance of GluR2 Mutant Mice

The GluR2 heterozygous (+/−) mice appeared healthy, well groomed, and fertile. The GluR2 homozygous mutants were born viable and showed no apparent abnormalities in general appearance until postnatal 2–3 weeks, when the mutant mice (n = 50) could be easily identified by their much smaller size and reduced weight (11.5 ± 0.8 gm in +/+ mice versus 6.5 ± 1.3 gm in −/− mice). In addition, depending on the litter size, ~20% of the mutants died at 2–3 weeks after birth. Both the growth retardation and mortality rate of the mutants were dramatically reduced by separating the littermates from the parents to reduce the litter size. Therefore, reduced feeding as a result of competition between littermates may contribute to an increased mortality rate in mutants. Mutant mice (including dying mice) showed no sign of seizure activity as measured by observation, EEG, or post-mortem analysis of pyramidal cell dropout in the hippocampus (data not shown). Surviving mutant mice recovered at 3 weeks of age, and by 6–7 weeks were similar to wild-type controls in both size and weight. Adult mutants appeared healthy and fully capable of caring for themselves. No apparent change in lifespan was observed up to 12 months of age. Behavioral analysis of 13 +/+ and 10 −/− mice showed that the lack of GluR2 expression significantly impaired novelty-induced exploratory activities in the open-field such as rearing (frequency in −/− mice, 0.1 ± 0.1 versus 2.2 ± 1.1 in +/+ mice; $p < .05$) and object exploration (frequency in −/− mice, 2.9 ± 1.3 versus 9.1 ± 1.9 in +/+ mice; $p < .02$), decreased self-directed behaviors including grooming (duration in −/− mice 3.3 ± 2 s versus 8.8 ± 1.9 in +/+ mice; $p < .006$), disrupted motor coordination (fall latency on rotorod at 15 rpm in −/− mice, 4.8 ± 0.9 s versus +/+, 28 ± 5; $p < 0.001$), and impaired eye closure reflexes to approaching objects (1 of 6 −/− mice versus 10 of 10 +/+ mice; $p < .001$).

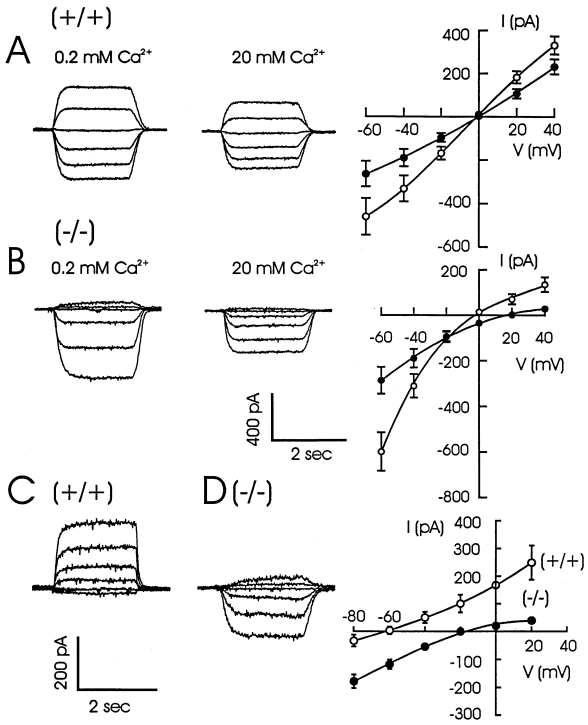

Figure 2. Enhanced Ca^{2+} Permeability in CA1 Neurons Lacking GluR2

(A) Representative kainate-evoked (100 μM) whole-cell currents for (+/+) neurons recorded in low (open circles) and high (closed circles) extracellular Ca^{2+}. The I/V relationships (right) for averaged steady-state currents from seven such neurons per condition. Curves were fitted by third to sixth order polynomials from which interpolated reversal potentials were calculated. Erev: −1.8 ± 1.3 mV and −1.0 ± 1.5 mV.

(B) Currents in mutant (−/−) neurons are illustrated, and averaged currents of seven such cells are also plotted.

(C and D) Recordings were also made in a solution containing 10 mM Ca^{2+} but lacking Na^{+}. Representative responses from (+/+) (C) and (−/−) (D) neurons are shown.

Relative Ca^{2+} Permeability in Neurons from GluR2 Mutant Mice

Currents evoked by the nondesensitizing agonist, kainate (Burnashev et al., 1992a), in isolated CA1 pyramidal neurons from wild-type mice exhibited little or no rectification, while their reversal potentials were insensitive to change from low to high extracellular Ca^{2+} (Erev: −1.8 ± 1.3 mV and −1.0 ± 1.5 mV [Figure 2A]). This suggests that most of the AMPARs in normal CA1 neurons contain the edited GluR2 subunit and have a low permeability to Ca^{2+}. Cells taken from mutant mice demonstrated both an enhanced inward rectification and a Ca^{2+}-dependent shift of the reversal potential (Erev) (Figure 2B), as predicted for the loss of the GluR2 subunit (Hollmann et al., 1991; Verdoorn et al., 1991; Geiger et al., 1995; Burnashev et al., 1995; Jonas et al., 1994). The Erev shifted from −4.1 ± 1.9 mV to 16.0 ± 2.3 mV, which indicates a substantial increase in Ca^{2+} permeability in mutant channels. In addition, the degree of inward rectification (Puchalski et al., 1994) of these currents was enhanced. The shift in the reversal potential for NMDA-evoked currents (n = 6) was similar (low Ca^{2+}, −2.0 ±

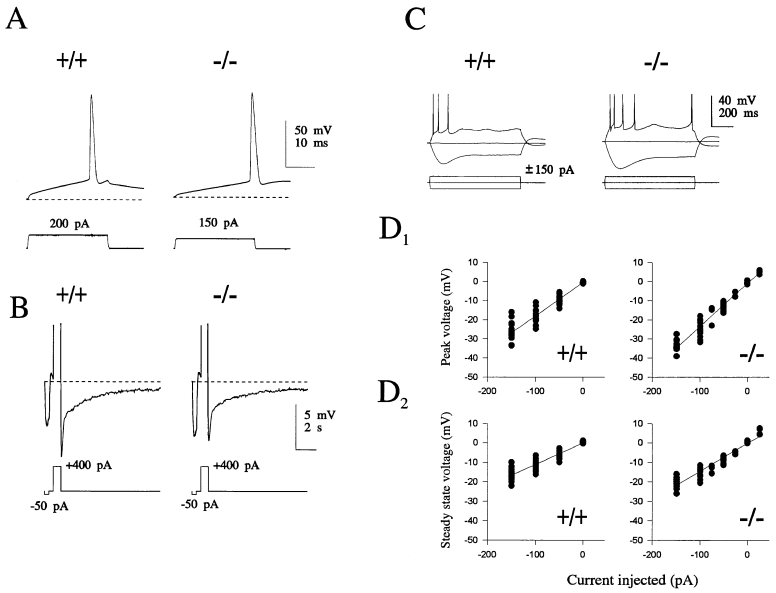

Figure 3. Passive Membrane Properties of Pyramidal CA1 Neurons from Hippocampal Slices

(A) Action potentials evoked by depolarizing current pulses.

(B) Post-spike-train afterhyperpolarization induced by 800 ms depolarizing current pulses, which generated 9–11 action potentials. A 50 pA current pulse preceeding the depolarizing pulse was used to test the membrane input resistance. Traces were averaged from responses of 16 control (+/+) and 14 GluR2 (−/−) mutant mice.

(C) This shows typical voltage response to current injection in one representative CA1 neuron for each group. Note that the action potential amplitudes are truncated. D_1 and D_2 summarize the I/V plots obtained from 17 control and 17 mutant neurons. D_1 represents peak voltage responses and D_2 represents steady-state voltage responses to 800 ms of hyperpolarizing current injection.

1.7 mV; high Ca^{2+}, 13.3 ± 2.3 mV) (data not shown). When the kainate-evoked currents were recorded in the presence of high extracellular Ca^{2+} and the absence of any extracellular monovalent cations, the relative permeability to Ca^{2+} was increased almost 9-fold in cells taken from GluR2 mutant mice (Figures 2C and 2D). Cells taken from wild-type mice demonstrated a significantly more negative Erev (−64.5 ± 4.7 mV, n = 6) than those taken from knockouts (−17.0 ± 2.2 mV, n = 5). Moreover, the calculated relative Ca^{2+} permeability (Burnashev et al., 1995) of currents in cells from knockout mice (P Ca^{2+}/P Cs^{+} = 3.51 ± 0.60) was significantly larger than that from wild type (P Ca^{2+}/P Cs^{+} = 0.41 ± 0.11).

Passive Membrane Properties

Whole-cell patch-clamp recordings from CA1 neurons in the slice (Figure 3) revealed no significant differences between control and mutant mice, respectively, in resting membrane potential (−64.8 ± 0.7 mV versus −63.5 ± 0.6 mV; p = 0.15), spike amplitude (114.9 ± 1.5 versus 111.9 ± 1.7 mV; p = 0.17), threshold to fire an action potential (−43.6 ± 0.8 versus −43.9 ± 0.89 mV; p = 0.75; Figure 3A), and area of afterhyperpolarization (AHP). Since the area of AHP is highly dependent on the number of action potentials induced by the depolarizing current, we limited our analysis to AHPs generated by a train of 9–11 action potentials evoked by 800 ms depolarizing current pulse (see Figure 3B). A typical post-spike-train AHP contains a fast and a slow component known as medium- (mAHP) and slow-duration AHP (sAHP; Storm, 1987). The amplitude of mAHP was −7.9 ± 0.6 mV and −5.4 ± 0.6 mV (p = 0.18), and the area of sAHP was 17,330 ± 2,881 mV.ms versus 18,396 ± 3,844 mV.ms (p = 0.5) in control and GluR2 mutants, respectively.

The membrane input resistance was significantly higher in GluR2 mutant mice (267 ± 10 MA) than that of control (190 ± 11 MA, p = 0.00001; see Figure 3D1). Such an increase in the membrane input resistance, in the absence of a change in the membrane potential, would suggest either reduced cell size or reduced dendritic arborization in the mutant animals. The anomalous rectification mediated by $C1^{-}$ current activation, and seen as a sag of hyperpolarizing responses exceeding −80 mV (Purpura et al., 1968; Halliwell and Adams, 1982), was not altered significantly (see Figures 3C and 3D2).

Presynaptic Mechanisms

In an attempt to study the efficacy of synaptic transmission in wild-type and GluR2 mutant animals, we compared the input-output curves in the CA1 subfield of hippocampal slices. The slope of field excitatory postsynaptic potential (fEPSP) was plotted versus presynaptic fiber volley amplitude, which is an index of presynaptic fiber excitability and results from the extracellular currents surrounding the synchronously activated unmyelinated fibers running in the dendritic layers. Since its amplitude is inversely proportional to the propagation distance (Andersen et al., 1978), the distance between recording and stimulating electrode was kept constant. As shown in Figure 5A, the efficacy of excitatory synaptic transmission in the hippocampal CA1 subfield was indistinguishable between the wild-type control and GluR2 mutant mice.

To test further for any abnormal presynaptic function, we investigated the differences in paired-pulse facilitation, which is an example of use-dependent increases in synaptic efficacy and is considered to be presynaptic in origin (Barrett and Magleby, 1976). In hippocampus, when two stimuli are delivered to the Schaffer collaterals in rapid succession, paired-pulse facilitation manifests itself as an enhanced dendritic response to the second stimulus as the interstimulus interval gets shorter. We did not observe any significant difference in the extent of the paired-pulse facilitation, over an interpulse interval range of 20 ms to 1 s, between slices obtained from control and GluR2 mutant mice (Figure 5B): at an interpulse interval of 50 ms, the magnitude of facilitation was 1.50 ± 0.03 (n = 20) and 1.49 ± 0.14 (n = 20) in

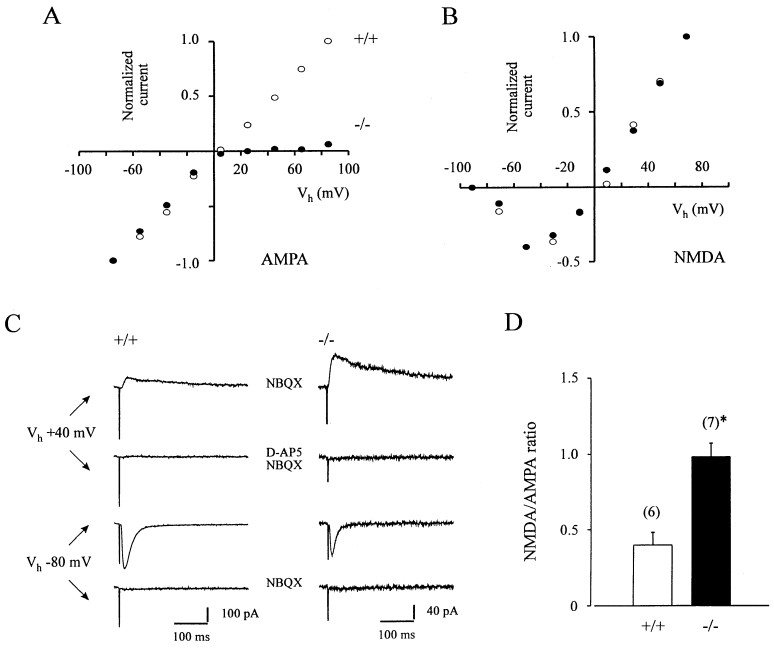

Figure 4. Whole-Cell Recordings of Evoked EPSCs in CA1 Neurons

(A) and (B) show a representative normalized I/V plot of AMPA and NMDA currents, from +/+ (n = 7) and −/− (n = 7) CA1 neurons. AMPA and NMDA currents were isolated by 50 μM AP5 and 5 μM NBQX, respectively, in the continuous presence of 10 μM BMI, and were normalized to their respective maximums.

(C) Representative traces of synaptic currents from a wild-type (+/+) and a mutant CA1 neuron (−/−) recorded in whole-cell voltage clamp in the presence of 10 μM BMI at a holding potential of +40 mV (upper two traces, NMDA component) and −80 mV (lower two traces, AMPA component). The first trace at V_h = +40 mV was recorded in the presence of 5 μM NBQX, which was subsequently blocked by addition of 50 μM D-AP5 (second upper trace). The first trace at V_h = −80 mV was recorded in the presence of 10 μM BMI, which was blocked by 5 μM NBQX.

(D) Summary histogram showing ratio of NMDA receptor channel current at +40 mV to synaptic currents at −80 mV, obtained from seven control (+/+) neurons and seven mutant (−/−) neurons.

control and GluR2 mutant slices, respectively. These data suggest that in GluR2 mutant mice, the excitability of Schaeffer collateral fibers and neurotransmitter release is likely to be normal.

Postsynaptic Mechanisms

Synaptic activity in hippocampal CA1 pyramidal cells, evoked by stimulation of Schaeffer collateral-commissural axons, was recorded by both extracellular field and whole-cell recordings. In extracellular field recordings, excitatory postsynaptic potentials (EPSPs) appeared to be normal in GluR2 mutant mice. D-AP5 (50–100 μM), a selective NMDA receptor antagonist, did not have a significant effect on the extracellular synaptic responses obtained at low frequency stimulation (LFS) in both control and GluR2 mutant mice, while NBQX (5 μM), an AMPA/kainate receptor antagonist, blocked all synaptic transmission in both the presence and absence of D-AP5. These results suggested that synaptic transmission at low frequency is predominantly AMPA mediated and that the lack of GluR2 subunit did not perturb synaptic transmission. However, since the amplitude of synaptic currents depends on the stimulus intensity, and stimulus intensities are not precisely comparable from slice to slice, we carried out whole-cell voltage-clamp recordings under conditions in which we minimized the number of synapses activated, by increasing the extracellular Ca^{2+} and magnesium concentration to 4 mM each, and reducing the stimulation intensity.

Whole-cell voltage-clamp data, recorded in the presence of both $GABA_A$- and $GABA_B$-mediated inhibitory postsynaptic currents (IPSCs), did not show any obvious difference among the cells obtained from wild-type control and GluR2 mutant slices (see Figure 4). The I/V relation of the NMDA component in neurons obtained from seven control and seven GluR2 mutant mice was not significantly different, thereby indicating that NMDA receptors have their usual voltage dependence (see Figure 4B). However, the I/V relation of the AMPA component was significantly different in the GluR2 mutant mice: in cells obtained from control animals, AMPA currents were quite linear, while those obtained from GluR2 mutant mice demonstrated a significant rectification at the positive holding potentials (see Figure 4A). The reduction of outward AMPA current at positive holding potentials is in agreement with previous reports obtained from cells lacking the GluR2 subunit (Hollmann et al., 1991; Verdoorn et al., 1991; Geiger et al., 1995; Koh et al., 1995a).

Figure 4C illustrates that in both control and GluR2 mutant mice, AMPA and NMDA components of evoked EPSCs were completely blocked by NBQX (5 μM) and D-AP5 (50 μM), respectively. The evoked synaptic EPSC, recorded in the presence of 10 μM BMI, is predominantly mediated by AMPAR activation at a holding potential of −80 mV (Clark and Collingridge, 1995; Spruston et al., 1995). There was no significant difference in the average synaptic current decay time constant at −80 mV (18.6 ± 3.1 ms in GluR2 mutant mice and 19.4 ± 2.3 ms in control mice; P = 0.85). The decay time constants of AMPAR-mediated EPSCs measured in CA1 neurons of both control and GluR2 mutant mice are similar to values reported by other groups under similar recording conditions (Kato et al., 1993; Perkel and Nicoll, 1993; Clark and Collingridge, 1995). The average decay time constant for the NMDA component, recorded in the presence of NBQX (5–10 μM) and at a holding potential of +40 mV, for control and GluR2 mutant mice, was 174.1 ± 20.5 ms and 166.3 ± 22.7 ms, respectively (P = 0.80).

The AMPA current amplitudes, measured 7 ms from stimulation artefact (Clark and Collingridge, 1995), were

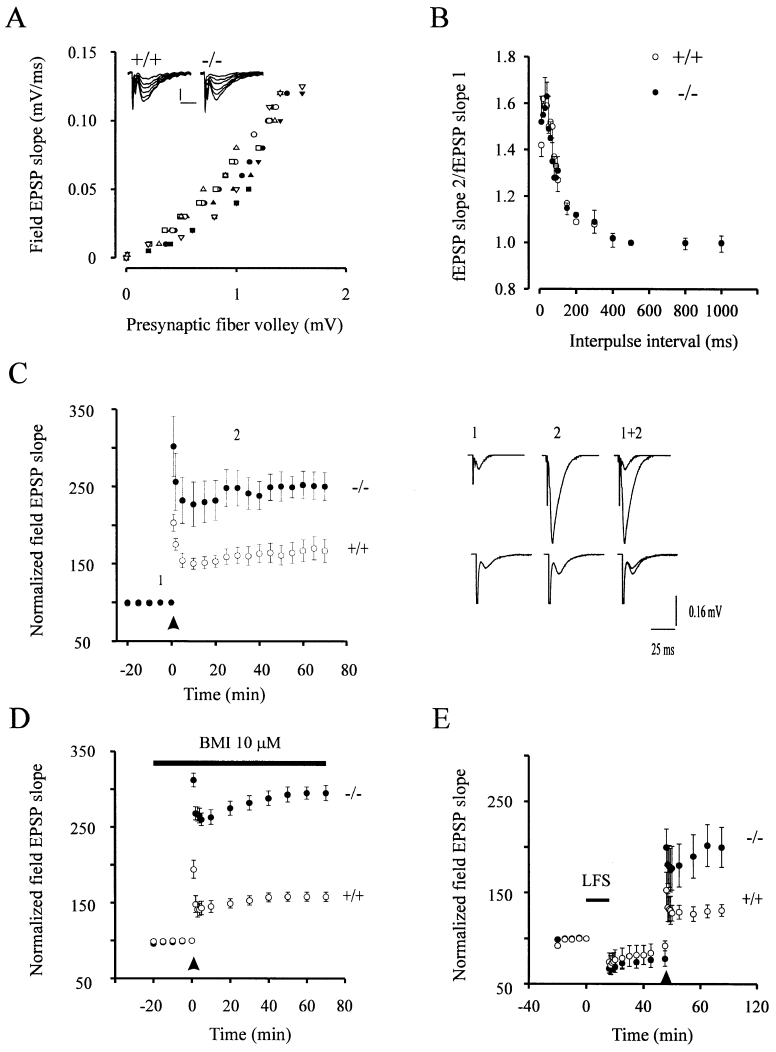

Figure 5. Synaptic Responses, LTP, and LTD in GluR2 Mutants

Synaptic responses in the CA1 subfield of hippocampal slices obtained from 15- to 30-day-old wild-type (+/+) and mutant (−/−) GluR2 littermates.

(A) Initial slopes of fEPSPs plotted as a function of presynaptic fiber volley amplitude. Each symbol represents a set of experiments from a single slice obtained from four mutants and four age-matched littermates from a single litter (+/+: open symbols; −/−: filled symbols). Inset traces show typical fEPSPs evoked with various stimulus intensities (calibration bars are 0.22 mV and 12.5 ms).

(B) Paired pulse facilitation in wild-type and mutant slices. The plot summarizes facilitation of the second fEPSP slope compared with the first one as a function of the interpulse interval (20 slices from ten +/+ and ten −/− mice). For (C), (D), (E), the data are plotted as the mean slope of the fEPSP ± SEM (normalized with respect to the 10 min immediately preceding the tetanus) versus time. The baseline stimulation intensity was 30%–50% of maximal response (30–80 μs) delivered at 0.03 Hz and was constant throughout the experiment. Tetanic stimulation (100 Hz for 200 ms delivered five times at 0.1 Hz) was given at arrows.

(C) LTP in the CA1 subfield of hippocampal slices, tetanized (arrow) in the absence of BMI in 20 slices, obtained from ten wild-type (open circles) or ten GluR2$^{-/-}$ (closed circles) mice. Right panel shows representative traces (averages of 10) at the times indicated by arabic numerals on the graph in (C).

(D) LTP in the presence of 10 μM BMI from 5 slices from five +/+ mice and 12 slices from ten −/− mice.

(E) Effects of LFS (1 Hz for 900 s) on potentiation induced by tetanic stimulation: four slices from three +/+ mice and eight slices from five −/− mice.

significantly smaller in neurons from GluR2 mutant mice than from their littermate control mice. To standarize and compare the evoked EPSC amplitudes between the two groups, we analyzed the ratio of NMDA to AMPA components in each group. The NMDA receptor–mediated EPSCs were obtained in the presence of 5 or 10 μM NBQX and at a holding potential of +40 mV. The NMDA current amplitudes were measured 100 ms from stimulation artefact (Clark and Collingridge, 1995). As shown in Figure 4D, there was a significant difference in the NMDA/AMPA ratio between the control and GluR2 mutant mice (0.40 ± 0.08 and 0.98 ± 0.09, respectively; $P = 0.0006$). The high NMDA/AMPA ratio of the mutant mice suggests that the postsynaptic AMPAR density may be reduced. This could occur if the remaining AMPAR subunits were not able to assemble effectively. This possibility is supported by the observation that the affinity of other AMPAR subunits is greater for GluR2 than for each other (Wenthold et al., 1996). Alternatively, the reduction in postsynaptic AMPAR density may be caused by reduced cell size or dendritic aborization, as mentioned earlier. If one assumes that both AMPA and NMDA receptor channels are colocalized postsynaptically, then one would expect a similar reduction in the NMDA components of the evoked EPSCs. The lack of any obvious reduction in the NMDA component of the evoked EPSCs argues against the latter hypothesis. Nevertheless, our data do provide some evidence that in the absence of GluR2 subunit, the other AMPAR subunits do form functional channels and carry out fast synaptic transmission.

Synaptic Plasticity

Long-term potentiation (LTP) in the CA1 subfield of hippocampal slices was studied in 16- to 30-day-old control and GluR2 mutant littermates both in normal (2 mM) and high (3.4 mM) Ca^{2+}-containing artificial cerebrospinal fluid (ACSF). We did not observe any significant differences in the magnitude of LTP obtained from GluR2 mutant hippocampal slices perfused in either normal or high Ca^{2+}-containing ACSF. However, slices obtained from control mice showed a higher failure rate in LTP induction when perfused with normal Ca^{2+}-containing ACSF. Hence, only data obtained from high Ca^{2+}-containing ACSF are reported. Tetanic stimulation (100 Hz for 200 ms delivered five times at 0.1 Hz) induced a long lasting (more than 2 hr) increase in the synaptic strength

in the control slices (Figure 5C). The normalized EPSP slope for control mice at 60 min after tetanus was 167% ± 15% of the average slope before stimulation (n = 20). In slices obtained from GluR2 mutants, the extent of long-lasting increase in the synaptic strength was enhanced by 2-fold. The normalized EPSP slope for GluR2 mutant mice at 60 min after tetanus was 252% ± 17.8% (P = 0.005) of the average slope before stimulation (n = 20). When tetanic stimulation was delivered in the presence of bicuculline (i.e., in the absence of GABAergic transmission), the magnitude of potentiation seen was indistinguishable from that obtained in the absence of bicuculline. At 60 min after tetanus, the normalized EPSP slope for the control and GluR2 mutant mice was 158% ± 5.9% (n = 5) and 295% ± 17% (n = 12; P = 0.0003), respectively (Figure 5D).

It was possible that neurons from GluR2 mutant mice were initially set at a more depressed level, and as a consequence of this set value, the tetanus-induced enhancement in synaptic efficacy was greater. To investigate this hypothesis, we first depotentiated the synapse and then induced LTP in both control and GluR2 mutant mice. Our data demonstrate that the magnitude of long-term depression (LTD) was not significantly different in control and GluR2 mutant mice, thereby suggesting that synapses in GluR2 mutant mice are not initially depressed. When averaged across slices, an initial transient depression following the standard LFS gave rise to a maintained LTD of 87.3% ± 7.2% (n = 4) in control slices and 82.6% ± 9.9% (n = 8; P = 0.752) in GluR2 mutant mice (Figure 5E). Furthermore, our data demonstrated that the magnitude of enhancement in synaptic efficacy from a depotentiated level is significantly different between control and GluR2 mutant mice (154.8% ± 10.3%, n = 4 and 268% ± 37.7%, n = 8; P = 0.03), respectively.

When the tetanic stimulation was delivered in the presence of 50–100 μM D-AP5, slices from control mice did not exhibit LTP, while those from GluR2 mice displayed a detectable residual LTP (normalized fEPSP slope at 60 min after tetanus was 154.8% ± 10.3%, n = 10; Figure 6A). This residual LTP in the presence of D-AP5 could be due to Ca^{2+} influx via the high voltage activated Ca^{2+} (HVAC) channels. However, when we induced LTP in the presence of D-AP5 and nifedipine (a HVAC channel antagonist), the normalized fEPSP slope at 60 min after tetanus was 132.7% ± 7.6% (n = 8), which was not significantly different from those recorded in D-AP5 alone (P = 0.05; Figure 6B). Hence, these results strongly suggest that GluR2 mutant mice have ~150% of enhancement in synaptic efficacy in the absence of NMDA and HVAC channel contribution. On the other hand, 5 μM NBQX or CNQX application, 20 min after tetanus, abolished all synaptic responses (Figure 6C), implying that the residual LTP in GluR2 mutant mice is likely mediated by the Ca^{2+} influx through the AMPARs.

LTP is a saturable phenomenon (Bliss and Collingridge, 1993). If the LTP induction mechanism in GluR2 mutant mice is not altered, one would expect to see saturation of LTP after a plateau is reached. However, Figure 6D shows that whereas LTP in slices from control mice saturates, those from GluR2 mutant mice can progressively produce more LTP until spreading depression

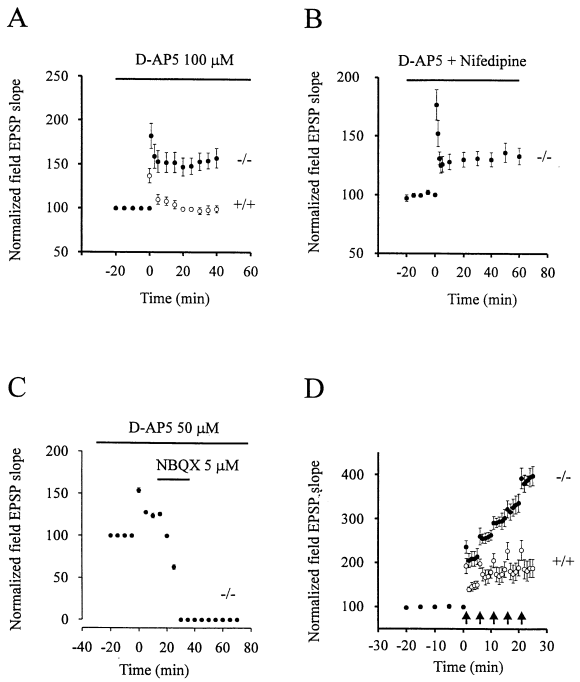

Figure 6. Enhanced NMDA-Independent LTP in GluR2-Deficient Mice

(A) GluR2-deficient mice exhibit NMDA-independent LTP. The plot summarizes LTP induced at time zero in the presence of 100 μM D-AP5 from five slices (five +/+ mice) and ten slices (five −/− mice).

(B) L-type, high voltage activated Ca^{2+} channels are not involved in the NMDA-independent LTP in GluR2 mutant mice. The plot summarizes LTP induced in the presence of 100 μM D-AP5 and 20 μM nifedipine in eight slices obtained from five GluR2-deficient mice.

(C) The NMDA-resistant component of LTP was blocked by 5 μM NBQX applied at 20 min after tetanus (n = 5).

(D) AMPA-mediated LTP does not saturate. Subsequent tetani were given at 5 min intervals (arrows) until saturation of LTP was obtained in control slices. The plot summarizes data obtained from 5 control and 12 mutant slices.

develops. In 12 slices obtained from GluR2 mutant mice, the normalized fEPSP slope measured 5 min after the first tetanus was 214% ± 18.2%, and that after the fifth tetanus was 397% ± 21.7%, whereas in 5 slices obtained from control mice, the normalized fEPSP slopes were 150% ± 8.6% and 188% ± 20.4%, respectively. These results, therefore, suggest that in GluR2 mutant mice, the mechanisms underlying LTP induction are modified.

Discussion

Our data are compatible with the suggestion that the Ca^{2+}-permeable AMPARs can induce LTP. Hence, in the absence of GluR2, both LTP and Ca^{2+} permeability are increased. Antagonists of AMPA and NMDA receptors block all the enhanced LTP seen in GluR2 mutant mice. The data also show that Ca^{2+} influx via L-type Ca^{2+} channels is not involved in LTP induction in GluR2 mutant mice. Therefore, the GluR2 subunit may play a crucial role in regulating both Ca^{2+} influx and LTP. The fact that GluR2 mutant mice exhibit widepsread impairment

in behavior suggests that GluR2 is also critical for normal brain function.

GluR Expression

The results suggest that we have created a null mutation in the GluR2 locus. The *neo*R gene inserted into exon 11 has stop codons in all three reading frames and a poly(A) site. No full-length GluR2 protein was seen in overloaded gels at a 1% level of detection. Although a short truncated GluR2 transcript could be made from exons 1–10, we detected no truncated GluR2 protein in 100-fold overloaded Western blots. Since the GluR2 antibody recognizes the N-terminus of the protein, it should have detected any protein made. However, we saw no extra band in the range of 1–200 kd on Western blots, not even a GluR–*neo* fusion. Likewise, an antibody with dual specificity for GluR3 and the C-terminus of GluR2, showed a loss of the comigrating GluR2 protein in GluR2 mutants. Finally, the 9-fold change in Ca^{2+} permeability in GluR2 $-/-$ neurons was in the range that would be predicted from the loss of GluR2 (Burnashev et al., 1995). Therefore, we likely have created a null mutation in the GluR2 locus. GluR2 loss itself might also alter the stoichiometry of GluR1, 3, and 4 assembly in the membrane, but this does not alter postsynaptic transmission, although AMPA responses were smaller in mutants.

Relative Ca^{2+} Permeability of AMPA Receptors

It has been shown in vitro that AMPARs containing the Q/R edited GluR2 subunit exhibit lower Ca^{2+} permeability and distinct gating properties, compared with receptor channels assembled without this subunit (Hollmann and Heinemann, 1994; Burnashev et al., 1992a). As expected, the loss of this GluR2 subunit in individual CA1 pyramidal neurons from GluR2 mutant mice demonstrated a 9-fold increase in relative Ca^{2+} permeability following kainate application, when compared with that of control mice. Indeed, this shift was similar in magnitude to that observed for Ca^{2+}-permeable NMDA receptors (Koh et al., 1995a). These results, together with observations in hippocampal slices from GluR2 editing–deficient mice (Brusa et al., 1995), support a crucial role for the GluR2 subunit in inhibiting Ca^{2+} influx via AMPARs in vivo.

GluR2 Subunit and Synaptic Plasticity

One could argue that enhanced synaptic plasticity seen in GluR2 null mutant mice was due to changes in either passive membrane properties, or the conductances for the inhibitory components of the synaptic response. However, our data indicate that there is no difference in either the passive membrane properties or the IPSCs among the slices obtained from control and GluR2 null mutant mice. One might also presume that Ca^{2+} influx through the AMPARs would be sufficient to block the Cl^- ionophore of the $GABA_A$ receptors (Inoue et al., 1986) and thereby give rise to the enhanced LTP. However, the magnitude of enhancement in synaptic strength was also the same under conditions where GABAergic transmission was blocked by bicuculline, suggesting that changes in the IPSCs are not the underlying mechanism for the enhanced synaptic efficacy observed in the GluR2 mutants.

The magnitude of the rise in postsynaptic Ca^{2+} during LTP induction, and the level of NMDA receptor function, have been shown to have significant effect on the generation of LTP (Malenka, 1991). Previous reports also showed that *trans*-ACPD, a metabotropic glutamate receptor agonist, enhanced NMDA receptor currents in CA1 cells and, when applied with a weak tetanus incapable of inducing LTP by itself, generated LTP (Aniksztejn et al., 1992; Bashir et al., 1993; O'Connor et al., 1994, 1995). Since NMDA receptor function is strongly modulated by kinase activity (Gerber et al., 1989; MacDonald et al., 1989; Chen and Huang 1991, 1992; Kelso et al., 1992; Yamazaki et al., 1992), it is conceivable that in GluR2 mutants the Ca^{2+} influx from AMPARs could modify the NMDA receptor function through protein phosphorylation or direct binding to calmodulin (Ehlers et al., 1996). However, this is unlikely, since in GluR2 mutant mice, whole-cell data did not reveal any change in the NMDA component of the synaptic current. Moreover, addition of NMDA-independent LTP in GluR2 mutants to NMDA-dependent LTP in control mice reconstituted the enhanced LTP seen in GluR2 mutants. In addition, LTD, another NMDA-dependent phenomenon, was not altered. These findings strongly support the hypothesis that Ca^{2+} influx, via AMPARs lacking the GluR2 subunit, is not modifying the NMDA component and is sufficient for producing LTP.

Several studies have suggested the presence of NMDA receptor–independent LTP in the CA1 Schaeffer collateral synapse. Perfusion of a high extracellular Ca^{2+} solution induces a long-lasting enhancement in the synaptic strength (Turner et al., 1982), which is not blocked by the NMDA receptor antagonist APV (Grover and Teyler, 1990a). NMDA receptor–independent LTP was also induced in CA1 by using a 200 Hz, rather than the usual 100 Hz tetanic stimulation (Grover and Teyler, 1990b). Postsynaptic injection of BAPTA, a Ca^{2+} chelator, or bath application of nifedipine, the dihydropyridine Ca^{2+} channel (L-type) antagonist, blocked this form of LTP, suggesting that in the presence of APV, HVAC channels provided the necessary Ca^{2+} influx required for LTP at the Schaeffer collateral synapse. Such a mechanism could underlie the NMDA receptor–independent enhancement in GluR2 mutants. However, when we perfused slices with nifedipine, in the presence of D-AP5, the residual LTP was unaffected, thereby indicating the lack of L-type HVAC channel involvement in NMDA-independent LTP in GluR2 mutant mice. Therefore, our data raise the possibility that Ca^{2+} influx via AMPARs devoid of GluR2 subunit is sufficient to induce LTP, in a NMDA-independent manner. A recent study on spinal cord neurons, where AMPA receptors are naturally devoid of the GluR2 subunits and are therefore Ca^{2+} permeable, showed that synaptic strength varied in an activity-dependent way (Gu et al., 1996). Furthermore, it is interesting to note that LTP in GluR2 mutant slices did not saturate, thus indicating that the mechanism(s) underlying LTP induction is altered. One reason for normal saturable LTP could be that Ca^{2+} influx through the NMDAR channel activates calmodulin, which is known to bind and inactivate the NMDAR1

Table 1. The Effect of Genetic Background on LTP

Strain	GluR2 Genotype	Number of Animals	LTP[a] (Mean)	Standard Error	Comparison p Value	
1. CD-1	+/+	n = 36	164	5	1 vs 2 NS	1 vs 5, $p < 0.001$
2. 129SV	+/+	n = 22	163	6	2 vs 3, $p < 0.001$	1 vs 4, NS
3. 129SV	−/−	n = 6	296	16	2 vs 5, $p < 0.001$	3 vs 5, NS
4. CD1 × 129F2	+/+	n = 36	169	4	2 vs 4, NS	3 vs 4, $p < 0.001$
5. CD1 × 129F2	−/−	n = 32	272	9	1 vs 3, $p < 0.001$	4 vs 5, $p < 0.001$

[a] Mean percent increase in fEPSP slope at 60 min after tetanus.
Post-hoc comparisons (SNK test; $\alpha = 0.05$) revealed a significant difference between two sets of means. Groups 3 and 5 were significantly different from groups 1, 2, and 4. No significant differences were found within each set. Abbreviations: NS, not significant.

channel (Ehlers et al., 1996). Therefore, normal LTP may be self-limiting. However, in GluR2$^{-/-}$ mice, the additional Ca^{2+} influx will not inactivate the AMPAR channel, thereby leading to an ever-increasing LTP at higher stimulation intensities. Alternatively, downstream signaling components may limit LTP in normal animals. In GluR2$^{-/-}$ mice, the additional Ca^{2+} could activate kinases that are normally rate limiting, to generate nonsaturable LTP.

Our data raise the possibility that activation of Ca^{2+} permeable AMPARs is sufficient to induce LTP; however, further experiments are needed to elucidate the mechanism(s) underlying this phenomenon. The generation of these GluR2 mutant mice provides one valuable model for determining the in vivo roles of the AMPARs and Ca^{2+} in synaptic physiology and behavior. Our results indicate that GluR2 is not required for LTP but seems to play a negative role in its regulation. Therefore, GluR2 may play an important role in synaptic plasticity by regulating its expression in development.

Experimental Procedures

Targeting Vector Construction

A genomic clone containing exons 7–12 of the GluR2 gene was isolated from a genomic 129 phage DNA library, prepared from R1 ES cells, after screening with rat GluR2 cDNA as a probe. Exon 11, containing TM1 and TM2, was sequenced, and the amino acid sequence deduced from DNA sequence was identical to the published mouse sequence in the corresponding region (Sakimura et al., 1990). The targeting vector was prepared by inserting a 1.8 kb HindIII–BglII fragment 5′ region to exon 11, and a 6.0 kb KpnI–BamHI fragment 3′ to exon 11 into the pPNT plasmid vector (Tybulewicz et al., 1991). The 1.8 kb HindIII–BglII was first subcloned into pBluescript vector (Stratagene) to obtain NotI and XhoI restriction sites. The 6 kb KpnI–BamHI fragment was cloned into pPNT by KpnI and blunt end ligation. The construct was designed to delete transmembrane region TM1 and the pore loop of exon 11. Therefore, a 0.4 kb BglII–KpnI fragment containing transmembrane domain (TM) 1 and 2 in exon 11 was replaced by a 1.8 kb fragment containing the PGK*neo* cassete carrying stop codons in all the reading frames and a poly(A) tail. A PGK-TK cassete was inserted downstream of exon 12 as a negative selection marker.

Generation of GluR2 Mutant Mice

The vector DNA was linearized with NotI restriction digestion and transfected into strain 129 ES cells of R1 line (Nagy et al., 1993) by electroporation (Bio-Rad, Gene Pulser, set at 240 V and 500 μF). G418 (150–250 μg/ml) and gancyclovir (2 μm) was applied 24 hr after transfection, and double resistant colonies were isolated during days 7–10 of selection. Genomic DNA of resistant clones was digested with BamHI and hybridized with a 0.5 kb DNA fragment 5′ to the HindIII–BglII fragment as an external probe (Figure 1A). Four clones (from a total of 1350 analyzed) were shown to contain desired targeted events, and all of them were used to produce chimeric mice via aggregation with CD1 morulae (Wood et al., 1993). The contribution of ES cells from the agouti 129 strain to the germline of chimerae was determined by mating with white CD1 mice and screening for agouti offspring. Germline transmission was confirmed by Southern blotting of tail DNA. Since only one ES clone transmitted the mutation through the germline, it is possible, although unlikely, that the phenotype we observe is due to an unintended mutation elsewhere in the genome of this clone. We intercrossed 129 × CD1 F1 mice heterozygous for the targeted mutation to homozygosity. Homozygous females and males were fertile, but very poor breeders. All experimental mice in Figures 1–6 included wild-type controls, heterozygotes, and homozygotes, which were littermate controls generated by heterozygous breeding of F1 to yield a 129 × CD1 F2 population. In larger experiments, mice from several litters were pooled, keeping a balanced number of −/−, +/−, or +/+ mice from each cage.

Three control experiments together show that the enhanced LTP in GluR2 mutant mice is due to the loss of GluR2 (Table 1). Analysis of variance revealed a significant difference between all groups ($F[4,126] = 67.4$; $p < 0.001$). A post-hoc Student Neuman–Keuls test ($\alpha = 0.05$) confirmed that the mutant groups (Groups 3 and 5) are not different from one another, but are significantly different from control groups 1, 2, and 4. No significant differences were found between the latter groups. We also performed multiple comparisions between groups using the Student's *t* test (two-tailed) with Bonferoni adjustment (Table 1). For example, LTP in the CA1 region of the parental 129 and CD1 strains showed no significant differences (Table 1). Therefore, the enhanced LTP seen in our genotyped GluR2$^{-/-}$ mice from the F2 cross could not be due solely to the inheritance of 129 genes conferring high LTP. To rule out the possibility that GluR2-linked 129 genes could contribute to the CA1-LTP phenotype in the context of a CD1 genetic background, we carried out experiments analyzing CA1 LTP distribution among an F2 population (n = 36) derived from wild-type F1 intercrosses (i.e., CD1 × 129). The frequency histogram showed that the distribution of LTP was normal ($p = 0.31$ Kolmogorov–Smirnov goodness-of-fit test). For the wild-type F2 129sv × CD1 population, there is 0.99 probability that a randomly chosen subject from the population will yield LTP between 118% and 218%. If single recessive wild-type CD1 and 129 genes interact in a simple way as to mimic the high LTP seen in GluR2$^{-/-}$ mice, we would have expected a bimodal distribution with 25% of the values above this LTP range. However, only one LTP score (260%), out of 36 obtained, was outside the estimated range (118–218). A one sample χ^2 goodness-of-fit test revealed a significant difference in the obtained ratio of high LTP (1/36) compared with the expected ratio (9/36), ($\chi^2 = 9.48$, $df = 1$; $p < 0.01$). This analysis argues against the possibility that single recessive genes interact in the background and contribute to enhanced LTP in GluR2$^{-/-}$ mice, but they do not rule out multiple gene effects. Finally, we have crossed our original 129 germline–derived chimeric male with 129, rather than CD1 mice (Table 1). Enhanced LTP was seen in GluR2$^{-/-}$ mice from several litters compared with +/+ ($p < .00001$). In this experiment, there is no possibility that CD1 background genes are playing any role, since they were not used in this cross. These results show that enhanced LTP is seen in the absence

of GluR2 on different genetic backgrounds. We feel these results together argue against the possibility that the genetic background is the only contributing factor in enhanced LTP in our GluR2$^{-/-}$ mice.

Western Blots

Three or more fresh brains from each GluR2 genotype (+/+), (+/−), or (−/−) mice were pooled, homogenized in 0.32 M sucrose, and centrifuged for 20 min at 2000 g, 4°C. The supernatant was transferred to 2 vol of water and centrifuged for 15 min at 5000 g. The pellet was resuspended in water using a polytron, and the centrifugation and resuspension steps were repeated twice more, resuspending the final pellet in 50 mM Tris–Cl (pH 7.0). The amount of total protein was assayed (Pierce), and the samples were diluted to 5 mg/ml protein, and used fresh or frozen at 70°C. These crude synaptic plasma membrane samples were prepared for polyacrylamide gel electrophoresis by the method of Laemmi. We ran 50 microgram samples on 8% gels, and the separated proteins were transferred to nitrocellulose membranes. The blotted proteins were probed with polyclonal anti-GluR1 (UBI); monoclonal anti-GluR2/4, which only recognized GluR2 on Western blots (Puchalski et al., 1994) (3A11 Pharmingen); polyclonal anti-GluR2/3 (UBI); polyclonal anti-GluR4 (UBI); polyclonal anti-GluR6/7 (UBI); polyclonal anti-NR1 (UBI) and polyclonal anti-NR2A/2B (generously provided by R. J. Wenthold, NIH). The blots were then probed with second antibodies linked to alkaline phosphatase or horseradish peroxidase, and the proteins visualized with the appropriate substrates for detection. To compare the amounts of receptors on some of the blots, enhanced chemiluminescence (Amersham) method of detection was utilized and the films were scanned for optical density (n = 3). GluR2 could be detected in gels loaded with 5, 50, or 500 mg of proteins using the 3A11 antibody. However, no band was detected in GluR2$^{-/-}$ mice in this range of protein concentrations. Therefore, its level of sensitivity is 1%.

Electrophysiology

Dissociated Hippocampal Neurons

Hippocampal neurons were mechanically isolated from slices of the CA1 region using 4 mg/ml papaya latex (Wang and MacDonald, 1995). Borosilicate patch electrodes (3–5 MΩ) were filled with the following: 140 mM CsF, 35 mM CsOH, 10 mM HEPES, 2 mM $MgCl_2$, 11 mM EGTA, 2 mM TEA, 1 mM $CaCl_2$, 2 mM MgATP (pH 7.3 using CsOH, 300 mosM). The low or high Ca^{2+} solutions contained the following: 140 mM NaCl, 0.2 or 20 mM $CaCl_2$, 5.4 mM KCl, 25 mM HEPES,33 or 13 mM glucose, 0.0005–0.001 mM TTX (pH 7.4 using NaOH, 320–335 mosM). The Na^+-free solution consisted of 10 mM $CaCl_2$, 25 mM HEPES with equiosmotic glucose or sucrose substituting for NaCl. Relative permeability ratios at 22°C were determined from the Erev recorded in Na^+-free solution using the constant field equation:

$$P_{Ca}/P_{CS} = [Cs^+]_i/[Ca^{2+}]_o \exp(EF/RT)[\exp(EF/RT) + 1]/4$$

where **E** is the reversal potential, and **F, R,** and **T** have their conventional meaning. P_{Ca} and P_{Cs} represent the permeability coefficients to Ca^{2+} and Cs^+.

Hippocampal Slices

400 μM thick hippocampal slices were obtained from 2- to 4-week-old wild-type or mutant mice. Slices were incubated in a storage chamber for 1 hr before transferring to an interface recording chamber. Both storage and recording solutions were oxygenated and contained in the following: 124 mM NaCl; 3 mM KCl; 1.25 mM NaH_2PO_4; 2 mM $MgSO_4$; 2 mM $CaCl_2$; 26 mM $NaHCO_3$; and 10 mM D-glucose. Solution for LTP studies contained the following: 124 mM NaCl; 3 mM KCl; 1.25 mM KH_2PO_4; 2.5 mM $MgSO_4$; 3.4 mM $CaCl_2$; 26 mM $NaHCO_3$; and 10 mM D-glucose. Electrophysiological recordings were carried out at room temperature (22°C–25°C) with the exception of LTP studies (32°C ± 0.5°C). Prior to 10 μM BMI perfusion, connections between CA3 and CA1 were cut. Field potential recordings in the CA1 region of hippocampus were performed with micropipettes filled with 1 M NaCl. Whole-cell recordings from CA1 cells were performed using the "blind method" (Blanton et al., 1990). For studies on the passive membrane properties of CA1 neurons, the internal pipette solution contained the following: 150 mM K_2MeSO_4; 0.1 mM EGTA–NaOH; 10 mM HEPES; 2 mM K–ATP (pH 7.2 adjusted with NaOH). Evoked EPSCs were recorded from CA1 cells with patch pipettes (4–7 MA), and the internal pipette solution contained the following: 130 mM Cs_2MeSO_4; 5 mM QX-314; 1 mM NaCl; 1 mM $MgCl_2$; 0.05 mM EGTA; 5 mM HEPES (pH 7.2, 280 mOsm). Synaptic currents and field potentials were evoked by placing a single glass electrode filled with either ACSF or 1 M NaCl. Responses were evoked at a frequency of 0.03 Hz and 0.07 Hz in field and whole-cell recordings, respectively. Tetani to evoke LTP consisted of five trains of 100 Hz stimulation lasting for 200 ms at an intertrain interval of 10 s. LTD was evoked by 900 stimuli at a frequency of 1 Hz. Current and field potentials were recorded using an Axopatch 200A and Axoclamp 2B amplifiers, respectively (Axon Instrument). Glass pipettes were fabricated from borosilicate glass with an optical density of 1.5 mm, and pulled with a two-step Narishige puller. The series resistance was 70%–96% compensated. Data were acquired on a 486-IBM compatible computer using PCLAMP6 software (Axon Instrument). The data were sampled at 5 kHz, and were subsequently digitally filtered during analysis. BMI was purchased from Sigma. D-AP5, CNQX, and NBQX were purchased from Trocris Neuramin. Data is expressed as mean ± SEM. Significance is tested using Student's *t* test. All experiments were carried out double blind.

Histochemistry

Mice were perfused with PBS (100 mM, pH 7.4) followed by 4% paraformaldehyde in PBS at 4°C. Whole brains were dissected from each perfused animal along with the cervical and lumbar spinal cord. Samples then were post-fixed 3 hr in 4% paraformaldehyde in PBS (0.1 M) and paraffin-embedded, or serial cryostat sections were obtained throughout the entire CNS in the horizontal, sagittal, or coronal planes. For each plane, two mice 30 days of age were analyzed for each genotype. To examine cellular morphology, ten μm paraffin sections were stained with thionine, or the brains were stained en block by the Golgi method, and compared with wild-type (+/+) sections previously obtained at the same level. No differences were found in cellular morphology between +/+ and −/− mice.

To analyze fiber tracts, thirty micron serial cryostat sections were taken in the sagittal plane from two 25-day-old postnatal GluR2 animals of each genotype (+/+, +/−, and −/−). Examination of every fourth section, by interference contrast microscopy, revealed no gross deviations in mutants in the origin, projection, or termination of the following tracts: anterior commissure (anterior and posterior projections); habenulo-interpeduncular tract (fusiculus retroflexus); stria medullaris; optic chiasma; mammilo-thalamic tract; fimbria fornix projections and posterior commissure. In addition, the layers of the olfactory bulb, cerebellum, and neocortex also appeared grossly normal. The corpus callosum and striatal structure exhibited normal proportions. In addition, all the associated nuclei of the cranial nerves, locus coeruleus, nucleus ruber, substantia nigra-reticulata, medullaris, striatum, optic chiasm, and tract appeared normal in the three genotypes.

Coronal serial sections (every tenth) were also examined for cytochrome C oxidase activity. This mitochondrial enzyme is located primarily on the dendrites and somata of postsynaptic cells and is a general reflection of the level of presynaptic input (Chiaia et al., 1992; Bates and Killackey, 1985). No differences were observed in the level of cytochrome C oxidase activity in GluRB$^{-/-}$ mice compared with control littermates.

Behavioral Analysis

For the open field test, mice were placed singly in a plastic box (46 × 25 × 15 cm) for a 5 min session, and their motor and posture patterns were recorded with an event recorder (Gerlai et al., 1993). GluR2 null mutant mice, or littermate controls, were measured for decreased frequency of visits to a novel object and locomotion scores. For the rotating rod test, each mouse was placed on a 3 cm diameter rod set at 15 rpm. The latency to fall off the rod was recorded (Gerlai, 1996). In the eye-closure test, mice were approached in their home-cage from above by a rubber rod, so that the rod was slowly moved toward their heads but stopped directly in front of them 1 cm away from their eyes. The behavioral responses were videotaped.

Acknowledgments

This work was supported by the Medical Research Council of Canada and the Ontario Mental Health Foundation. Zhengping Jia was a Networks of Centres of Excellence Neuroscience fellow and Nadia Agopyan was a Medical Research Council Centennial fellow. We thank S. Heinemann for the GluR2 cDNA clone, Y. M. Lu for some of the data in Table 1, and C. Janus for statistical analysis.

The costs of publication of this article were defrayed in part by the payment of page charges. This article must therefore be hereby marked *"advertisement"* in accordance with 18 USC Section 1734 solely to indicate this fact.

Received June 18, 1996; revised September 19, 1996.

References

Andersen, P., Silfvenius, H., Sundberg, S.H., Sveen, O., and Wingstrom, H. (1978). Functional characteristics of unmyelinated fibers in the hippocampal cortex. Brain Res. *144*, 11–18.

Aniksztejn, L., Otani, S., and Ben-Ari, Y. (1992). Quisqualate metabotropic receptors modulate NMDA currents and facilitate induction of long term potentiation through protein kinase C. Eur. J. Neurosci. *4*, 500–505.

Barrett, E.F., and Magleby, K.L. (1976). Physiology of the cholinergic transmission. In Biology of Cholinergic Function, (A.M. Goldberg and I. Hanin, eds. (New York: Raven Press), pp. 29–100.

Bashir, Z.I., Bortolotto, Z.A., Davies, C.H., Beretta, N., Irving, A.J., Seal, A.J., Henley, J.M., Jane, D.E., Watkins, J.C., and Collingridge, G.L. (1993). Induction of LTP in the hippocampus needs synaptic activation of glutamate metabotropic receptors. Nature *363*, 347–349.

Bates, S.C.A., and Killackey, H.P. (1985). The organization of the neonatal rat's brainstem trigernimal complex and its role in the formation of central trigernimal pattersn. J. Comp. Neurol. *240*, 265–287.

Blanton, M., Lotorco, J., and Kreigstein, A. (1990). Whole-cell recording from neurons in slices of reptilian and mammalian cortex. J. Neurosci. Meth. *30*, 203–210.

Bliss, T.V.P., and Collingridge, G.L. (1993). A synaptic model of memory: long-term potentiation in the hippocampus. Nature *361*, 31–39.

Bowie, D., and Mayer, M.L. (1995). Inward rectification of both AMPA and kainate subtype glutamate receptors generated by polyamine-mediated ion channel block. Neuron *15*, 453–462.

Brusa, R., Zimmerman, F., Koh, D.S., Feldmeyer, D., Gass, P., Seeburg, P.H., and Sprengel, R. (1995). Early-onset epilepsy and postnatal lethality associated with an editing-deficient GluR-B allele in mice. Science *270*, 1677–1680.

Burnashev, N., Monyer, H., Seeburg, P.H., and Sakmann, B. (1992a). Divalent ion permeability of AMPA receptor channels is dominated by the edited form of a single subunit. Neuron *8*, 189–198.

Burnashev, N., Khodorova, A., Jonas, P., Helm, P.J., Wisden, W., Monyer, H., Seeburg, P.H., and Sakmann, B. (1992b). Ca^{2+} permeable AMPA/KA receptors in fusiform cerebellar glial cells. Science *256*, 1566–1570.

Burnashev, N., Zhou, Z., Neher, E., and Sakman, B . (1995). Fractional Ca^{2+} currents through recombinant GluR channels of the NMDA, AMPA and kainate receptor subtypes. J. Physiol. (Lond.) *485*, 403–418.

Chen, L., and Huang, L.Y.M. (1991). Sustained potentiation of NMDA receptor–mediated glutamate responses through activation of protein kinase C by a μ opioid. Neuron *7*, 319–326.

Chen, L., and Huang, L.Y.M. (1992). Protein kinase C reduces Mg^{2+} block of NMDA receptor channels as a mechanism of modulation. Nature *356*, 521–523.

Chiaia, N.L., Bennett-Clarke, C.A., and Rhoades, R.W. (1992). Differential effects of peripheral damage on vibrissa-related patterns in trigernimal nucleus principalis subnucleus interpolaris and subnucleus candidates. Neuroscience *49*, 141–156.

Clark, K.A., and Collingridge, G.L. (1995). Synaptic potentiation of dual component excitatory postsynaptic currents in the rat hippocampus. J. Physiol. (Lond.) *482*, 39–52.

Dingledine, R., Hume, R.I., and Heinemann, S.F. (1992). Structural determinant of barium permeation and rectification in non-NMDA glutamate receptor channels. J. Neurosci. *12*, 4080–4087.

Ehlers, M.D., Zhang, S., Bernhardt, J.P., and Huganir, R.L. (1996). Inactivation of NMDA receptors by direct interaction of calmodulin with the NR1 subunit. Cell *84*, 746–755.

Geiger, J.R.P., Melcher, T., Koh, D.S., Sakman, B., Seeburg, P.H., Jonas, P., and Monyer, H. (1995). Relative abundance of subunit mRNAs determines gating and Ca^{2+} permeability of AMPA receptors in principal neurons and interneurons in rat CNS. Neuron *15*,193–204.

Gerber, G., Kangrga, I., Ryu, P.D., Larew, J.S.A., and Randic, M. (1989). Multiple effects of phorbol esters in the rat spinal dorsal horn. J. Neurosci. *9*, 3606–3617.

Gerlai, R. (1996). Gene targeting studies of mammalian behaviour: is it the mutation or the background genotype? Trends Neurosci. *19*, 177–189.

Gerlai, R., Friend, W., Becker, L., O'Hanlon, R., Marks, A., and Roder, J. (1993). Female transgenic mice carrying multiple copies of the human gene for S100β are hyperactive. Behav. Brain Res. *55*, 51–59.

Grover, L.M., and Teyler, T.J. (1990a). Effects of extracellular potassium concentration and postsynaptic membrane potential on Ca^{2+} induced potentiation in area CA1 of rat hippocampus. Brain Res. *506*, 53–61.

Grover, L.M., and Teyler, T.J. (1990b). Two components of long term potentiation induced by different patterns of afferent activation. Nature *347*, 477–479.

Gu, J.G., Albuquerque, C., Lee, C.J., and MacDermott, A.B. (1996). Synaptic strengthening through activation of Ca^{2+} permeable AMPA receptors. Nature *381*, 793–796.

Halliwell, J.W., and Adams, P.R. (1982). Voltage-clamp analysis of muscarinic excitation in hippocampal neurones. Brain Res. *250*, 71–92.

Hollmann, M., and Heinemann, S. (1994). Cloned glutamate receptors. Ann. Rev. Neurosci. *17*, 31–108.

Hollmann, M., Hartley, M., and Heinemann, S. (1991). Ca^{2+} permeability of KA-AMPA glutamate receptor channels depends on subunit composition. Science *52*, 81–85.

Hume, I.R., Dingledine, R., and Heinemann, S.F. (1991). Identification of a site in glutamate receptor subunit that controls Ca^{2+} permeability. Science *253*, 1028–1031.

Inoue, M., Oomura, Y., Yakushiji, T., and Akaike, N. (1986). Intracellular Ca^{2+} ions decrease the affinity of the GABA receptor. Nature *324*, 156–158.

Jonas, P., Racca, C., Sakman, B., Seeburg, P.H., Monyer, H. (1994). Differences in Ca^{2+} permeability of AMPA-type glutamate receptor channels in neocortical neurons caused by differential GluR-B subunit expression. Neuron *12*, 1281–1289.

Kamboj, S.K., Swanson, J.T., and Cull-Candy, S.J. (1995). Intracellular spermine confers rectification on rat calicum-permeable AMPA and kainate receptors. J. Physiol. *486*, 297–303.

Kato, K., Clifford, D.B., and Zorumski, C.F. (1993). Long term potentiation during whole cell recordings in rat hippocampal slices. Neuroscience *53*, 39–47.

Kelso, S.R., Nelson, T.E., and Leonard, J.P. (1992). Protein kinase C–mediated enhancement of NMDA currents by metabotropic glutamate receptors in *Xenopus* oocytes. J. Physiol. (Lond.) *449*, 705–718.

Koh, D.S., Geiger, J.R.P., Jonas, P., and Sakman, B. (1995a). Ca^{2+} permeable AMPA and NMDA receptor channels in basket cells of rat hippocampal dendate gyrus. J. Physiol. *485*, 383–402.

Koh, D.S., Burnashev, N., and Jonas, P. (1995b). Block of native Ca^{2+}-permeable AMPA receptors in rat brain by intracellular polamines generates double rectification. J. Physiol. *486*, 305–312.

MacDonald, J.F., and Wojtowicz, J.M. (1982). The effect of L-glutamate and its analogues upon the membrane conductance of central murine neurones in culture. Can. J. Physiol. Pharmcol. *60*, 282–296.

MacDonald, J.F., Mody, I., and Salter, M.W. (1989). Regulation of N-methyl-D-aspartate receptors revealed by intracellular dialysis of murine neurons in culture. J. Physiol. (Lond.) *414*, 17–34.

Malenka, R.C. (1991). Postsynaptic factors control the duration of synaptic enhancement in area CA1 of the hippocampus. Neuron *6*, 53–60.

Nagy, A., Rossant, J., Nagy, R., Abramow-Newerly, W., Roder, J.C. (1993). Derivation of completely cell culture–derived mice from early-passage embryonic stem cells. Proc. Nucl. Acids. Res. *90*, 8424–8428.

Nowak, L., Bregestovski, P., Ascher, P., Herbet, A., and Prochiantz, A. (1984). Magnesium gates glutamate-activated channels in mouse central neurones. Nature *307*, 462–465.

O'Connor, J.J., Rowan, M.J., and Anwyl, R. (1994). Long-lasting enhancement of NMDA receptor–mediated synaptic transmission by metabotropic glutamate receptor activation. Nature *367*, 557–560.

O'Connor, J.J., Rowan, M.J., and Anwyl, R. (1995). Tetanically induced similar increase in the AMPA and NMDA receptor components of the excitatory postsynaptic current: investigations of the involvement of mGlu receptors. J. Neurosci. *15*, 2013–2020.

Perkel, D.J., and Nicoll, R.A. (1993). Evidence for all-or-none regulation of neurotransmitter release: implications for long term potentiation. J. Physiol. (Lond.) *471*, 481–500.

Puchalski, R.B., Louis, J.C., Brose, N., Traynelis, S.F., Egebjerg, J., Kukekov, V., Wenthold, R.J., Rogers, S.W., Lin, F., Moran, T., Morrison, J.H., and Heinemann, S.F. (1994). Selective RNA editing and subunit assembly of native glutamate receptors. Neuron *13*, 131–147.

Purpura, D.P., Prelevic, S., and Santini, M. (1968). Hyperpolarizing increase in membrane conductance in hippocampal neurones. Brain Res. *7*, 310–312.

Sakimura, K., Bujo, H., Kushiya, E., Araki, K., Yamazaki, M., Yamazaki, M., Meguro, H., Warashina, A., Numa, S., Mishina, M. (1990). Functional expression from cloned cDNAs of glutamate receptor species responsive to kainate and quisqualate. FEBS Lett. *272*, 73–80.

Silva, A., Stevens, L.F., Tonegawa, S., and Wang, Y. (1992). Deficient hippocampal long-term potentiation in α-Ca^{2+}-calmodulin kinase II mutant mice. Science *257*, 201–206.

Sommer, B., Kohler, M., Sprengel, R., and Seeburg, P.H. (1991). RNA editing in brain controls a determinant of ion flow in glutamate gated channel. Cell *67*, 11–19.

Spruston, N., Jonas, P., and Sakman, B. (1995). Dendritic glutamate receptor channels in rat hippocampal CA3 and CA1 pyramidal neurons. J. Physiol. *482*, 325–352.

Storm, J.F. (1987). Action potential repolarization and a fast afterhyperpolarization in rat hippocampal pyramidal cells. J. Physiol. (Lond.) *385*, 733–759.

Turner, R.W., Baimbridge, K.G., and Miller, J.J. (1982). Calcium induced long term potentiation in the hippocampus. Neuroscience *7*, 1411–1416.

Tybulewicz, V.L., Crawford, C.E., Jackson, P.K., Bronson, R.T., and Mulligan, R.C. (1991). Neonatal lethality and lymphopenia in mice with a homozygous disruption of the C-abl photo-oncogene. Cell *65*, 1153–1163.

Verdoorn, T.A., Burnashev, N., Monyer, H., Seeburg, P.H., and Sakman, B. (1991). Structural determinants of ion flow through recombinant glutamate receptor channels. Science *252*, 1715–1718.

Wang, L.-Y., and MacDonald, J.F. (1995). Modulation by Mg^{2+} of the affinity of NMDA-receptors for glycine in murine hippocampal neurons. J. Physiol. *486*, 83–95.

Wenthold, R.J., Petralia, R.S., Blahos II, J., and Niedzielski, A.S. (1996). Evidence for multiple AMPA receptor complexes in hippocampal CA1/CA2 neurons. J. Neurosci. *16*, 1982–1989.

Wood, S.A., Allen, N.D., Rossant, J., Auerbach, A., and Nagy, A. (1993). Non-injection methods for the production of embryonic stem cell embryo chimeras. Nature *365*, 87–89.

Yamazaki, M., Mori, M., Araki, K., Mori, K.J., and Mishina, M. (1992). Cloning, expression and modulation of a mouse NMDA receptor subunit. FEBS Lett. *300*, 39–45.